APL Materials

Understanding the interplay of stability and efficiency in A-site engineered lead halide perovskites

Cite as: APL Mater. **8**, 070901 (2020); https://doi.org/10.1063/5.0011851
Submitted: 27 April 2020 . Accepted: 08 June 2020 . Published Online: 08 July 2020

Feray Ünlü, Eunhwan Jung, Jinane Haddad, Ashish Kulkarni, Senol Öz, Heechae Choi, Thomas Fischer, Sudip Chakraborty, Thomas Kirchartz, and Sanjay Mathur

Understanding the interplay of stability and efficiency in A-site engineered lead halide perovskites

Cite as: APL Mater. 8, 070901 (2020); doi: 10.1063/5.0011851
Submitted: 27 April 2020 • Accepted: 8 June 2020 •
Published Online: 8 July 2020

Feray Ünlü,[1] Eunhwan Jung,[1] Jinane Haddad,[2] Ashish Kulkarni,[2] Senol Öz,[3,4] Heechae Choi,[1] Thomas Fischer,[1] Sudip Chakraborty,[5] Thomas Kirchartz,[2,6] and Sanjay Mathur[1,a)]

AFFILIATIONS

[1]Institute of Inorganic Chemistry, University of Cologne, Greinstr. 6, 50939 Cologne, Germany
[2]IEK5-Photovoltaics Forschungszentrum Jülich, 52425 Jülich, Germany
[3]Saule Technologies, Dunska 11, 54-427 Wroclaw, Poland
[4]Saule Research Institute, Dunska 11, 54-427 Wroclaw, Poland
[5]Materials Theory for Energy Scavenging (MATES) Lab, Discipline of Physics, Indian Institute of Technology (IIT) Indore, Simrol, Indore 453552, India
[6]Faculty of Engineering and CENIDE, University of Duisburg-Essen, Carl-Benz-Str. 199, 47057 Duisburg, Germany

[a)]**Author to whom correspondence should be addressed:** sanjay.mathur@uni-koeln.de

ABSTRACT

Organic–inorganic hybrid lead halide perovskites have gained significant attention as light-harvesting materials in thin-film photovoltaics due to their exceptional optoelectronic properties and simple fabrication process. The power conversion efficiency of perovskite solar cells (PSCs) has surged beyond 25% in a short time span. Their transition to commercial market is a "work in progress" due to limited long-term operational stability and the persisting environmental concern due to the presence of lead. Comprehensive investigations on the interplay of material composition and interfacial effects on the device performance of PSCs based on methylammonium lead iodide have shown the crucial role of an A-site cation in incipient deterioration of the material through external stimuli (moisture, light, oxygen, or heat). Consequently, a partial or complete replacement of A-site cations by up to four isoelectronic substituents has resulted in many new perovskite compositions. The correlations between the chemical composition and the optoelectronic properties are, however, not always easy to determine. A-site cation management is governed by stability and charge neutrality of the lattice, and the choices include Cs^+-cations and organic cations such as $CH_3NH_3^+$ or $CH(NH_2)_2^+$ and combinations thereof. Since the size of the cations is an important structural parameter, an adequate compositional engineering of the A-site could effectively optimize the stability by reducing non-radiative defect sites and enhancing carrier lifetimes. This Perspective reflects on the experimental strategies for A-site cation management and their direct impact on the stability and device performance. It also highlights the opportunities and challenges for further research and industrial commercialization of PSCs.

INTRODUCTION

The growing need for renewable energy resources has put back research on photovoltaic materials on the forefronts of current solar cell technologies with focus lying on cost-effective production of electricity from solar power, when compared to the first generation silicon-based technology. In this context, solution-based light-harvesting technologies such as dye sensitized solar cells (DSSCs), organic photovoltaics (OPV), and perovskite solar cells (PSCs) have attracted significant attention due to their relatively inexpensive fabrication cost and expected short energy payback times.[1] In particular, the incorporation of perovskites

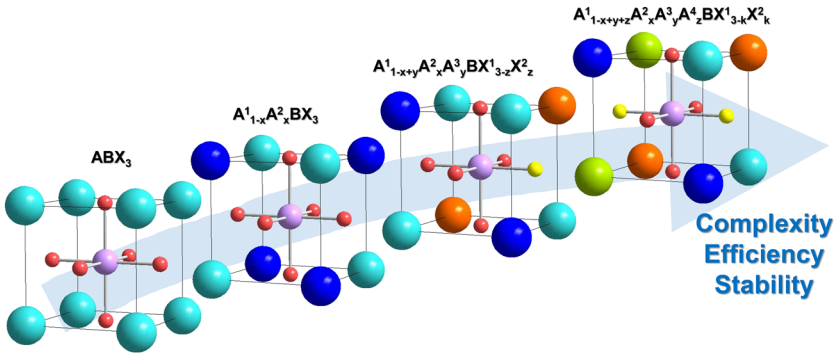

FIG. 1. A-site cation engineering in ABX_3 perovskites leading to more complex, stable, and highly efficient perovskite solar cells while structural composition and chemical composition are not well understood yet. **A**-site cations (turquoise, blue, green, and orange) representing monovalent cations are located at the corners of the **B**-centered unit cells, where B (violet) is Pb and **X** (red, yellow) is I (or Br).

as efficient solar absorbers enabled a breakthrough for emerging photovoltaics culminating in photoconversion efficiencies (PCEs) exceeding 25%.[2,3] These materials are represented by the well-known general formula ABX_3, where A is a pure organic or inorganic cation or a combination thereof, B is a central metal cation, and X is a halide anion. Nevertheless, the desired transition of the laboratory research data obtained at the level of individual or few cells to a technological module-level scale should address the common requirements such as cost, efficiency, and stability.[4] The exceptional optoelectronic properties, such as suitable bandgap,[5,6] low exciton binding energy (~2 meV to 50 meV),[5,7–9] long charge carrier diffusion lengths,[10,11] and ambipolar charge mobility,[12] make perovskites ideally suitable as solar absorbers. The easy modulation of processing conditions, composition, and device configuration leaves substantial unexplored experimental space for compositional engineering that is reflected in the scattering of optoelectronic properties of the reported materials. Among hybrid organic–inorganic perovskites, methylammonium lead iodide ($MAPbI_3$) is the most widely explored composition, which demonstrated photovoltaic efficiencies beyond 20%.[13–16] However, $MAPbI_3$ based photovoltaic devices degrade when exposed to environmental stimuli such as atmospheric moisture, heat, oxygen, and light that are detrimental for the nominal power output and consistent photoconversion efficiency.[17,18] For instance, in the case of $MAPbI_3$, the hygroscopic organic cation is liberated from the crystal structure mainly under exposure to moisture,[17] oxygen, and light,[19–21] thereby transforming photo-active $MAPbI_3$ into photo-inactive constituents and releasing toxic lead-iodide into the environment. The long-term stability is further affected by a phase transition from tetragonal to cubic occurring at 54 °C–57 °C,[22,23] which lies within the operation window and surface temperature observed in solar cells (up to 80 °C) and is responsible for diminishing the thermal stability of PSCs.[18,23,24] An increased thermal stability[25] achieved by substitution of MA with FA (or Cs^+) is accompanied by a reduced phase stability,[26–28] manifesting the trade-off of compositional engineering. Despite scattering in data and claims, there is a consensus that the ability of perovskite-based solar cells to perform efficiently over longer times is affected by both materials and device considerations, which need to be addressed from an industrial perspective to facilitate their deployment and commercial uptake. From the viewpoint of fundamental insights, compositional engineering of A-site cations is considered a viable strategy to offset material instabilities. In addition to the above-mentioned small organic cations or inorganic cations leading mostly to a three-dimensional perovskite structure, lower dimensional structures such as Ruddlesden–Popper phases or 2D/3D mixtures can be designed for stability. For instance, incorporating bulky organic cations, such as butylammonium (BA), phenylethylammonium (PEA), or ammonium valeric acid (AVA), along with MA (mixed-cation approach) has been demonstrated as an effective way to enhance the long-term stability of the perovskite solar cells while maintaining the device efficiency.[29–31]

This Perspective article highlights the recent advancements in compositional tuning of three-dimensional halide perovskites through partial replacement and multi-cation substitution of A-site in the ABX_3 lattice, resulting in organic–inorganic mixed-cation perovskites. Over the past few years, more complex compositions of organic–inorganic perovskites have been realized in order to achieve highly efficient and long-term stable absorber materials for PV device applications (Fig. 1). However, the addition of ions, all competing for the same crystallographic site in the perovskite structure, can also trigger unwanted effects such as local clustering, lattice strain, vacancies, and anti-site defects;[32–35] all of these cause inferior optoelectronic properties that need to be investigated in more detail. Therefore, we introduce the perovskite crystal structure and its properties shortly and then focus on the A-site cation engineering and how it affects and improves stability, efficiency, and opto-physical properties. Additionally, we work out prospects and opportunities for further research toward commercial applications.

PEROVSKITE STRUCTURE AND PROPERTIES

It is well-known that the structural stability of the perovskite absorber material depends mainly on certain crystallographic parameters and geometric constraints, which provides an understanding of factors governing the perovskite crystal lattice essential for any compositional changes. Named after the calcium titanate ($CaTiO_3$) mineral perovskite, discovered in 1839 by Gustav Rose and named in honor of the Russian mineralogist *Lew Alexejewitsch Perovski*, the perovskite crystal structure describes a family of crystalline compounds with cubic symmetry of the general chemical stoichiometry ABX_3, where A and B denote independent crystallographic sites, occupied by positively charged cations, while X positions are occupied by negatively charged anions to maintain charge neutrality. The technological importance of the perovskite

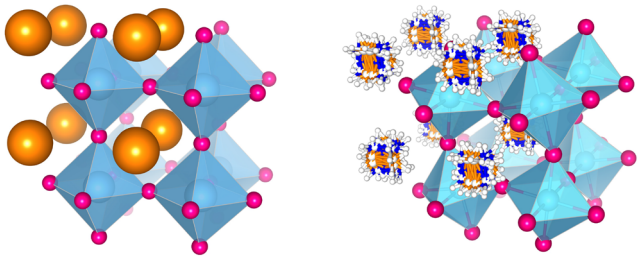

FIG. 2. The ideal cubic perovskite structure ABX_3 having a three-dimensional network of corner sharing $[BX_6]$ octahedra surrounding a larger A-site cation (left). The distorted perovskite lattice in $MAPbI_3$ with disordered organic MA-cations in A-site position (right).

structure arises due to its compositional flexibility that allows facile intermixing of suitable cation or anion combinations at the A-site ($A^1_{1-x}A^2_xBX_3$), B-site ($AB^1_{1-x}B^2_xX_3$), X-site ($ABX^1_{3-x}X^2_x$), or even at all three possible sites at once ($A^1_{1-x}A^2_xB^1_{1-y}B^2_yX^1_{3-z}X^2_z$), resulting in different optical (e.g., absorption and photoluminescence), electrical (e.g., photoconductivity, resistivity, and mobility), and electronic properties (e.g., band structure and bandgap). While the large A-site cations occupy the corners of the unit cell, the smaller sized B-site cations (B < A) occupy the center of the unit cell, and the X-site anions are located at the center of the faces, forming an octahedron with the central B-site cation (Fig. 2). Each unit cell is connected via the corner sharing octahedra to build a cubo-octahedral cage around the A-site cation.

The crystallographic stability and possible crystal structure can be deduced by considering an empirically derived tolerance factor t,[36] which is defined as the ratio of the distance A–X to the distance M–X in an idealized solid-sphere model with ionic radii R by

$$t = \frac{(R_A + R_X)}{\left(\sqrt{2}R_M + R_X\right)} \quad (1)$$

and an octahedral factor μ,[37] which is defined as the following ratio:

$$\mu = \frac{R_M}{R_x}. \quad (2)$$

For halide perovskites (X = F, Cl, Br, and I), the tolerance factor and octahedral factor vary between $0.81 < t < 1.11$ and $0.44 < \mu < 0.90$, respectively.[37] If t lies in the narrower range of $0.89 < t < 1.0$,[38] the cubic structure is likely to be stabilized, whereas tetragonal or orthorhombic structures are formed at $0.71 < t < 0.9$,[38] and higher $t > 1$[38] results in hexagonal non-perovskite structures that are not photo-active. Previous reports have shown that the observed optical bandgap is inversely proportional to the Goldschmidt tolerance factor in the range of $0.8 < t > 1.0$ for A-site variation, which can be used to engineer optical properties by careful selection of cation combinations.[36,39,40]

The optoelectronic properties of the hybrid organic–inorganic halide perovskite compounds are strongly determined by the inorganic metal-halide framework. The valence band consists of the s-lone pair of Pb^{2+} and halide p-orbitals, and the conduction band consists of lead 6p and halide p-orbitals (Fig. 3).[41] The Pb–X framework is distorted by the A-site cation through steric and Coulombic interactions, causing an octahedral tilting, which is responsible for the changes in the electronic structure near the band edges. The shape, size, and charge distribution of A-site cations govern the perovskite structure. For instance, the incorporation of a small amount of methyl ammonium ($CH_3NH_3^+$, MA) stabilizes the black α-phase of a formamidinium ($[CH(NH_2)_2^+$, FA] based perovskite leading to photoconversion efficiencies beyond 20%.[42]

STABILITY IN PEROVSKITES: A HIERARCHICAL CHALLENGE

The majority of commercial PV systems are based on silicon technology preferred due to high and stable device efficiencies up to 26.7%[3] and a lifetime warranty of up to 20 years[43] reproducibly achievable by established and standardized technological routes. On the other hand, perovskite-based solar cells demonstrate peak PCEs (>80% of theoretical maximum of 30% related to a bandgap of

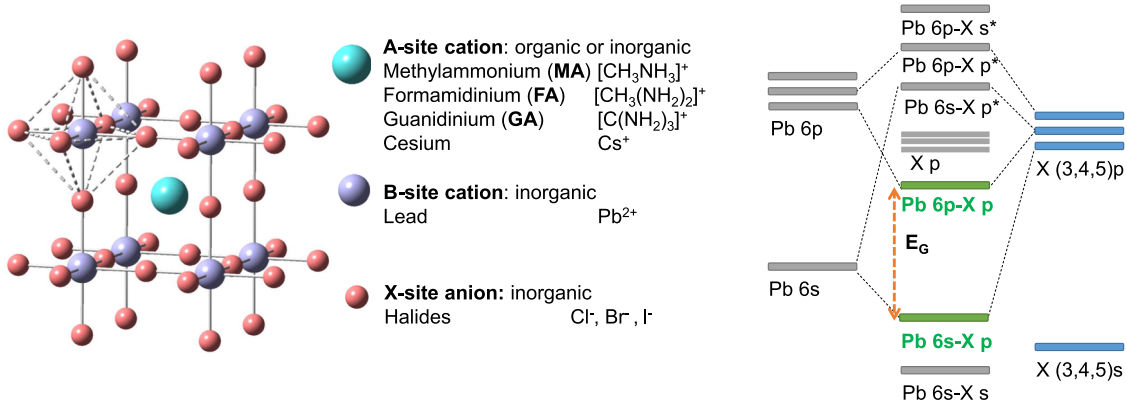

FIG. 3. The electronic structure of the ideal $APbX_3$ perovskite (left): the valence band (bottom green) consists of s (Pb) and p (halide) orbitals, and the conduction band (top green) consists of Pb and halide p orbitals, leading to a direct bandgap (E_G) (right).

1.6 eV[44]) within less than 10 years of development but are still limited to lab-scale devices (cell level) with an absorber area of typically <1 cm^2. Intrinsic and extrinsic stability issues hinder the widespread technological implementation of perovskite absorbers. Extrinsic stability issues, mainly caused by humidity and oxygen diffusion, can be targeted by established encapsulation methods. However, intrinsic factors originating from the chemistry of the absorber material itself, e.g., thermal instability and ion migration, explain the complex interdependence of material properties and device fabrication challenges.[45]

In order to penetrate into the PV-market, the PSC technology needs to demonstrate similar stability and efficiency relative to conventional PV products. Besides assuring sufficiently stable power conversion efficiencies, thorough understanding of degradation mechanisms at material, cell, and system levels is crucial for transferring the research understanding to a marketable product. Moreover, the complete technological value chain, from cradle to cradle in a circular economy, such as large-scale production methods, adoption of standardized test protocols, and handling and recycling of toxic substances are equally important parameters for possible industrialization of PSC technology. For example, the so-called hysteresis of perovskite solar cells, an electric field dependent photovoltaic conversion efficiency, is one known specific problem for unstable efficiencies.[46,47] A-site cation engineering has shown to be an appropriate method to overcome intrinsic stability issues and hysteresis. The polymorphism and thermal stability can be controlled by partial substitution of the A-site cation to stabilize the desired photo-active crystalline phases, to tune optical properties, and achieve sufficient thermal stability. In the following sections ("Compositional engineering for improved stability and efficiency" and "Compositional engineering for reduced recombination losses"), recent results obtained on the mixing of different A-site cations for achieving configurational stability in hybrid perovskites are presented.

COMPOSITIONAL ENGINEERING FOR IMPROVED STABILITY AND EFFICIENCY

Single-cation perovskites

The lack of phase stability casts a shadow over the excellent optical properties of $MAPbI_3$ with a record PCE of 21.6%,[13] due to the structural transition from the tetragonal to cubic phase at 54 °C–57 °C,[22,23] which leads to defects, lower charge carrier mobility, decreased diffusion length, and change in the band structure, followed by recombination losses in the absorber material.[34,48] In contrast, formamidinium (FA) based perovskites [$CH(NH_2)_2PbI_3$, $FAPbI_3$] undergo phase transition above 130 °C from the non-photo-active yellow hexagonal δ-phase to the photo-active black cubic or trigonal α-phase.[49] $FAPbI_3$ has a lower bandgap (1.47 eV[50] compared to 1.6 eV[51] n $MAPbI_3$) with a red-shifted absorption edge, enabling increased photoabsorption and power conversion efficiencies. Recently, Zhang *et al.*[52] obtained 21.07% PCE for $FAPbI_3$ solar cells based on the $FAPbI_3$ powder, which can be synthesized from a less pure lead iodide precursor. Furthermore, the formation of the δ-phase could be suppressed by this powder method approach, thus improving the stability of the device. In addition, all-inorganic perovskites such as $CsPbI_3$ are also used in solar cell applications despite their higher bandgap energy (1.73 eV) as they exhibit a high thermal stability exceeding 300 °C for the desired photo-active cubic α-phase.[53] Wang *et al.*[54] showed the effect of a dimethyl ammonium iodide (DMAI) additive on the crystallization of $CsPbI_3$, which stabilized the photo-active β-phase and γ-phase, and a PCE of 19.03% was obtained for β-$CsPbI_3$ with a passivation layer of PEA. The otherwise unstable phases of the pristine perovskites $MAPbI_3$, $FAPbI_3$, and $CsPbI_3$ can be stabilized through an increase in the configurational entropy,[55–57] which enlarges the perovskite complexity.

Double-cation perovskites

The compositional flexibility of the perovskite crystal structure enables substitution in the anion, as well as the cation sub-lattice. As both methylammonium (MA) and formamidinium (FA) are quite sensitive to ambient conditions causing phase instability, mixed A-site occupation with MA-cations and FA-cations produced hybrid perovskites with a stabilized crystal lattice and expanded absorption range due to the lowered bandgap.[58] Single phase double-cation black perovskite $(MA)_x(FA)_{1-x}PbI_3$ was synthesized via a sequential deposition method, where a PbI_2 thin-film was sequentially dipped into an alcoholic solution of the organic cations.[58] The addition of 20 mol. %–40 mol. % FA was shown to induce a red shift in the absorption edge while simultaneously maintaining the high absorption coefficient, typical for $MAPbI_3$, reaching the PCE values of 14.9% [Fig. 4(a)].[58]

Apart from the instability of the black α-phase of $FAPbI_3$ at room temperature forming a wide bandgap (yellow) hexagonal δ-phase, the organic–inorganic hybrid perovskites, although stabilized with MA-cations, have shown low photostability and thermal stability, due to the volatile and acidic (pK_a = 8.94)[59] MA organic moiety.[48,60] Due to an insufficient difference in ionic radii between MA and FA, the MA-cation initiated crystallization of α-$FAPbI_3$ perovskite occurs at a much slower rate than the smaller Cs^+-cation, thereby leaving a significant amount of the yellow phase untransformed.[61] For example, $Cs_{0.2}FA_{0.8}PbI_3$ was found to crystallize into the black phase already at room temperature.[56] Incorporation of smaller cesium-cations resulted in a shrunken cubo-octahedral A-site vacancy and, hence, a stronger interaction between the A-site cation and the iodide atoms manifested itself through the compressed unit cell dimensions (Vegard's rule).[62] Furthermore, the Cs^+ incorporation leads to larger perovskite grains, lower trap densities, and longer charge carrier lifetimes, improving the solar cell performance up to 17.1%, when compared to pristine $FAPbI_3$ with a PCE of 16.3%.[62] Recently, Li *et al.*[63] further improved the PCE of $Cs_{0.1}FA_{0.9}PbI_3$ using a zwitterion additive. $FAPbI_3$ has an ideal tolerance factor of 0.99, assuming a spherical ionic radius. However, the large FA-cation has a flat shape structure, which will lead to a higher tolerance factor, and a stable non-perovskite hexagonal phase is formed.[40] $CsPbI_3$ has a smaller tolerance factor (0.81); thus, in both cases, the formation of a stable cubic perovskite at room temperature is prevented.[40] However, partial occupation of both cations shifted the tolerance factor to a range, where the cubic perovskite structure could be stabilized, which can be understood by introducing the concept of a so-called effective tolerance factor [Fig. 4(b)].[40] Here, the effective radius is defined as follows:

$$r_{effective} = xr_{A1} + (1-x)r_{A2}\,, \tag{3}$$

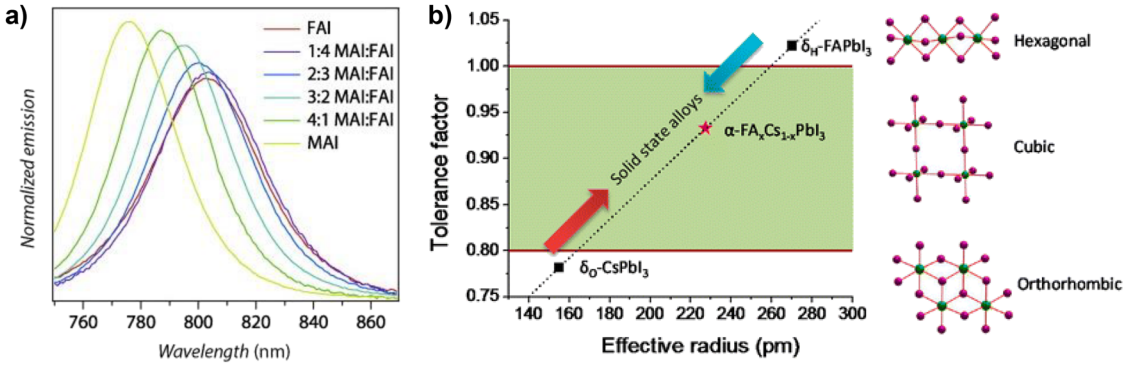

FIG. 4. (a) Emission peaks of different double-cation perovskites with varied MAI/FAI ratios; FAI containing perovskites show a red shift. Reprinted with the permission from Pellet *et al.*, Angew. Chem., Int. Ed. **53**, 3151 (2014). Copyright 2014 WILEY. (b) Effective tolerance factor for FA and Cs perovskite alloy to obtain a stable cubic perovskite phase. Reprinted with the permission from Li *et al.*, Chem. Mater. **28**, 284 (2016). Copyright 2016 American Chemical Society.

and the effective tolerance factor then follows through

$$t_{effective} = \frac{r_{effective} + r_X}{\sqrt{2}(r_{Pb^{2+}} + r_X)}. \quad (4)$$

In general, this approach can be used to identify new perovskite compositions that show enhanced photostability and thermal stability. In addition, bandgap engineering is also possible by mixing Cs^+ and FA to achieve wider bandgaps for tandem applications, which have been demonstrated with semi-transparent FA/Cs^+ mixed perovskites as suitable absorbers in Si-tandem solar cells.[64] Perovskite/Si tandem cells can theoretically achieve efficiencies up to 32.4% for a perovskite with a bandgap of 1.55 eV.[65] The ideal perovskite bandgap for a maximum efficiency of 45.1% would be 1.74 eV for a series two-terminal modules measured under standard test conditions (AM1.5G, 1 kW/m^2, 25 °C) calculated by Futscher and Ehrler via a detailed-balance limit.[65] Experimentally, a PCE of 29.1% was achieved for the two-terminal monolithic perovskite/Si tandem cell.[2]

Partial substitution with even smaller rubidium- (Rb^+-) cations also stabilizes the active black phase of $FAPbI_3$, while pure $RbPbI_3$ only crystallizes in the photo-inactive δ-phase (orthorhombic non-perovskite structure).[73] However, Park *et al.*[73] reported that the smaller ionic radius of the rubidium-cation affects the perovskite crystal structure of $FAPbI_3$ more strongly. X-ray diffraction (XRD) and differential scanning calorimetry (DSC) data revealed that Rb^+ inclusion leads to a favorable phase transition from yellow δ-$FAPbI_3$ to black α-$FAPbI_3$. In addition, by fluorescence lifetime image microscopy (FLIM), $Rb_{0.05}FA_{0.95}PbI_3$ was confirmed to exhibit a longer photoluminescence (PL) lifetime compared to pristine $FAPbI_3$, due to suppression of the yellow phase of $FAPbI_3$.[73] The best performing solar cells provided a stable operation for 1000 h under ambient conditions at an average relative humidity (RH) of 55% and 25 °C, maintaining 97% of the initial PCE. On the other hand, solid-state NMR spectroscopy data suggested that Rb^+ does not form an alloy with the FA perovskite, which is observed in the case of Cs^+ being incorporated into the $FAPbI_3$ lattice.[74] Rubidium halides rather acted as a passivation layer, thus reducing the defect density at the grain boundaries. Further attempts to stabilize $MAPbI_3$ or $FAPbI_3$ were also made by introducing small amounts of the larger guanidinium-cation [$C(NH_2)_3^+$, GA] into the host lattice,[75,76] which enhances thermal stability ($GA_{0.25}MA_{0.75}PbI_3$ keeps 90% of PCE for up to 300 h at 85 °C under argon, whereas $MAPbI_3$ keeps 70% of PCE under the same conditions[76]), due to an increased number of H–I bonds interacting with the inorganic framework. The improvement of H-bonding is also assumed to enhance the grain size and charge carrier transport at the interface and further passivation of undercoordinated iodine within the grain boundaries.[77]

Triple-cation perovskites

Theoretically, it is possible to improve the solar cell efficiency up to 33% for a single-junction perovskite solar cell depending on the bandgap, which was calculated by Shockley and Queisser.[78] The detailed balance Shockley–Queisser limit for the best performing single junction solar cell can be nearly obtained for bandgaps between 1.1 eV and 1.43 eV.[79] Among double-cation perovskites, best efficiencies (>20%) could be reached by FA/MA mixing (Table I).[42] Although this double-cation strategy already addresses some of the aforementioned obstacles, introducing cesium as the third A-site cation further enhances the device performance significantly. The smaller Cs^+-cation (1.81 Å) can be used in small amounts to influence the crystal structure by obtaining a decreased effective tolerance factor, which leads to a cubic or pseudo-cubic perovskite structure.[61] Hence, the desired photo-active phase is obtained at room temperature due to entropic stabilization.[56] Saliba *et al.*[61] developed the first solar cells based on a triple-cation perovskite with mixed halides $Cs_x(MA_{0.17}FA_{0.83})_{(1-x)}Pb(I_{0.83}Br_{0.17})_3$. Cs^+ can effectively suppress the yellow phase impurities of $FAPbI_3$ accomplishing enhanced and defect-free perovskite thin-films, leading to stabilized PCEs (up to 1000 h) exceeding 21%. The triple-cation perovskite is thermally more stable compared to the FA/MA perovskite, as well as more robust against environmental fluctuations such as different preparation protocols, temperatures, and solvent vapors. This thermal and environmental stability is one key factor for achieving higher operational reliability in perovskite solar cells, crucial for their large-scale application. Furthermore, Singh and Miyasaka[80] confirmed this outstanding stability (up to 18 weeks) of triple-cation

TABLE I. Some examples for A-site cation engineering from the literature. Tolerance factors were calculated using Eq. (4).

Perovskite	t	Bandgap (eV)	Phase	PCE (%)	References
$MAPbI_3$	0.91	1.55	Tetragonal	21.6	13
$FAPbI_3$	0.99	1.47	Trigonal	21.07	52
$CsPbI_3$	0.81	1.73	Tetragonal	19.03	54
$FA_{0.1}MA_{0.9}PbI_3$	0.92	1.54	Cubic	20.2	66
$(FAPbI_3)_{0.92}(MAPbBr_3)_{0.08}$	0.98	1.53	Not reported	23.4	42
$(FAPb_3)_{0.95}(MAPbBr_3)_{0.05}$	0.98	1.51	Trigonal	22.7	67 and 68
$FA_{0.9}Cs_{0.1}PbI_3$	0.95	1.52	Cubic	18.9	63
$Cs_{0.05}(MA_{0.17}FA_{0.83})_{0.95}Pb(I_{0.83}Br_{0.17})_3$	0.99	1.62	Cubic	21.1	69
$Rb_{0.05}(Cs_{0.05}MA_{0.17}FA_{0.83})_{0.95}Pb(I_{0.83}Br_{0.17})_3$	0.98	1.63	Not reported	20.6	70
$K_{0.035}(Cs_{0.05}MA_{0.15}FA_{0.85})_{0.95}Pb(I_{0.85}Br_{0.15})_3$	0.98	1.65	Not reported	20.56	71
$GA_{0.015}Cs_{0.046}MA_{0.152}FA_{0.787}Pb(I_{0.815}Br_{0.185})_3$	0.97	1.62	Cubic	20.96	72

perovskites fabricated under ambient conditions with a controlled relative humidity of 25% to achieve a stabilized PCE of >20%.

Multiple-cation perovskites

The further enlargement of perovskite complexity by the inclusion of additional cations, e.g., quadruple-cation hybrid perovskites, can be employed to enhance the already achieved stability and charge carrier transport optimizations. For example, it was shown that adding Rb^+ as the fourth cation in a Cs/FA/MA mixed halide perovskite stabilizes the absorber material even further possibly due to the increased oxidation resistance of alkali metal ions.[70] Matsui *et al.*[81] obtained PCEs over 18%, and 74% of PCE was retained at 85 °C under full illumination for up to 350 h, while without Rb^+, 50% of PCE was retained. With potassium incorporation in the quadruple-cation perovskite $K_xCs_{0.05}(FA_{0.85}MA_{0.15})_{0.95}Pb(I_{0.85}Br_{0.15})_3$, devices with a PCE of 20.56% for a small active area and 15.76% for 6 × 6 cm^2 modules [Fig. 5(a)] without hysteresis could be achieved.[71]

The incorporation of alkali metals to the triple-cation perovskite, where these occupy interstitial sites at the surface rather than in the crystal lattice, could show reduced hysteresis and reduced ion migration depending on the size, especially for potassium.[82] Abdi-Jalebi *et al.*[83] presented that potassium doping enhances the radiative efficiency, better than rubidium, and that rubidium forms large halide crystals, which is even accelerated under humidity (>30%), dropping down the performance compared to K^+.

In their recent work on the quadruple-cation perovskite $GA_{0.015}Cs_{0.046}MA_{0.152}FA_{0.787}Pb(I_{0.815}Br_{0.185})_3$, Jung *et al.*[72] showed that the inclusion of guanidinium- cations [$C(NH_2)_3^+$, GA] in the perovskite passivates the grain boundaries of thin-films to minimize the non-radiative charge carrier recombination at grain boundaries and enhances the non-radiative recombination time due to the suppressed formation of halide vacancies [Fig. 5(b)]. Moreover, the high pK_a value (13.6) of GA-cation hinders any deprotonation process that makes the perovskite very stable (70% of PCE was retained under ambient atmosphere at 80 °C for 60

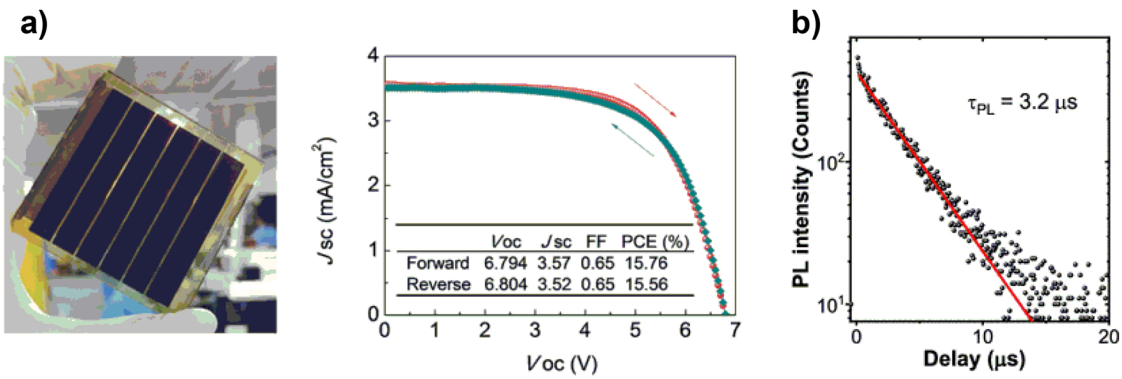

FIG. 5. (a) 6 × 6 cm^2 solar module of K^+ containing a quadruple-cation perovskite with >15% PCE. Reprinted with the permission from Bu *et al.*, Energy Environ. Sci. **10**, 2509 (2017). Copyright 2017 Royal Society of Chemistry. (b) Time resolved PL for GA containing quadruple-cation perovskite showing a PL lifetime of 3.2 μs. Reprinted with the permission from Jung *et al.*, ACS Energy Lett. **5**, 785 (2020). Copyright 2020 American Chemical Society.

days).[72,84] Also, quintuple-cation perovskites, using Rb^+-, K^+-, Cs^+-, FA-, and MA-cations, were reported in flexible perovskite solar cells achieving reduced recombination, less hysteresis, and high efficiency (19%).[85]

UNDERSTANDING THE INTERPLAY OF THE CHEMICAL STRUCTURE AND STABILITY IN MIXED-CATION PEROVSKITES

Compositional variation at the A-site has significantly advanced perovskite research reflected in enhanced efficiency and phase stability achieved through configurational engineering. Usually, multiple-cation and halide perovskites are made from a solution mixture of different precursors, which contain up to six different precursors for the fabrication of quadruple-cation perovskites, deposited via spin-coating or other solution-based methods to give solid thin-films. Although the effect of compositional changes on the absorption and charge transport properties has been extensively investigated,[48,72,86–88] relatively little attention has been devoted to fundamental studies on the chemical structure of perovskites based on mixed-cation compositions. Despite the predominant role of solution-based techniques, the nucleation and crystal growth in a solution and effects of grain growth and grain boundary defects have received less attention. Since these factors are decisive in achieving high efficiency, stability, and reproducibility at the device level, the resulting local microscopic composition of the resulting film is crucial for the maturation of PSC technology. In fact, several reports present contradictory data concerning the occupancy of the earth alkali metals. For instance, although confirmed by the XRD data, K^+- and Rb^+-cations have been reported to occupy the A-sites,[88] and subsequent works claim that both Rb^+ and K^+ ions segregate at the grain boundaries and passivate surface traps,[87] which was further substantiated by the ^{133}Cs, ^{87}Rb, ^{39}K, ^{13}C, and ^{14}N solid-state magic angle spinning (MAS) NMR study of double-cation, triple-cation, and quadruple-cation lead halides.[74,89] Macroscopically, an improvement in crystallinity and charge transport properties after the introduction of earth alkali metal cations in triple-cation and quadruple-cation perovskites has been observed. A triple coordinated intermediate structure involving Pb^{2+}, DMSO, and Cs^+ was identified, which enhances crystallization of perovskite thin-films with larger grains and fewer defects, thus improving V_{oc} and FF, as well as reproducibility under inert and ambient conditions.[90] Jian *et al.*[91] investigated the role of Cs^+-cations in triple-cation perovskites via *ab initio* molecular dynamic calculations. They observed that the arrangement of Cs^+-cations in the lattice leads to changes in the electronic structure and to stabilization of the Pb–I framework due to distortions.

Core level spectroscopy in several mixed-cation perovskite thin-films revealed that the double-cation MA/FA perovskite contains an excess of PbI_2 in bulk and formamidinium iodide (FAI) at the surface.[92] Further substitution of A-site cations, i.e., by using CsI or RbI, reduced the excess PbI_2 toward the bulk of the thin-film [Fig. 6(a)], whereas the remaining FAI was found at the surface, due to increased reactivity of RbI and CsI with PbI_2. In contrast to Rb^+, Cs^+ was found to be distributed homogenously in the bulk of a triple-cation perovskite. In case of a quadruple-cation perovskite (MA, FA, Cs, and Rb), PbI_3, Rb^+, and Cs^+ were homogenously distributed; however, the amount of unreacted organic cations found at the surface correlated with an increase in the substitution rate of A-site cations [Fig. 6(a)].

For double-cation perovskites, for example, Binek *et al.*[49] have showed that 15% of a MA-cation is sufficient to stabilize the α-phase at low temperature, as the intercalation of the small cation MA with a high dipole moment enhances the hydrogen bonding to the inorganic Pb–I cage. Moreover, increased stability with no phase separation can be attributed to better Coulomb interactions between the MA and Pb–I octahedra, which increases the Madelung energy [Fig. 6(b)].

These findings reveal that the desired ideal composition in multiple-cation perovskites is not fully achieved due to the presence of unreacted species. Single-phase solid solutions containing five or more components are known to be stabilized by the increasing configuration entropy (also known as mixing entropy).[93] However, by increasing the number of constituents, a high entropy mixture forms multiple phases depending on the temperature and reaction time. Very recently, the effect of the entropy, enthalpy, temperature, and number of the mixed elements on the phase stability of the mixture was investigated by Luan *et al.* using density functional theory (DFT) methods to unravel the underlying mechanism of phase formation of these high entropy mixtures in order to predict stable phases at room temperature.[94] The group showed that for high entropy intermetallic alloys with five constituents, the portion of the single phase without phase separation of other species is lower than 1% at room temperature due to more possible combinations of elements when increasing their number. Therefore, in the case of multiple-cation perovskites, it is vital to analyze the structure and phase-stability in order to understand the composition dynamics in solution and the subsequent formation of crystals, grains, and grain boundaries to fabricate highly efficient solar cells reproducibly. For mixed halide perovskites based on Cs^+- or MA- cations, there are several theoretical investigations concerning the crystal composition. A phase diagram of $MAPb(I_{1-x}Br_x)_3$ built on the Helmholtz free energy variation indicates the thermodynamic stability of the mixed-anion phases for different halide ratios at various temperatures [Fig. 6(c)] and explains the observed phase separation under illumination.[95] Local temperature inhomogeneities facilitate phase separation under illumination, which is slow at room temperature.[96–98] However, directly relating these observations to experiments remains difficult, as the final stoichiometry of the solid materials is usually not investigated in detail.

The fundamental understanding of formability, crystallization, and grain boundary engineering in A-site modified hybrid lead iodide perovskites is crucial. Within the perovskite lattice, the A-site cation fills the hollow space formed by eight corner-sharing $[PbI_6]$-octahedra and balances the charge of the entire network. Any variation in A-site cation size alters the structural parameters (tolerance and octahedral factors) affecting phase transitions, change in dimensionalities, and optoelectronic properties. Therefore, better understanding of processes such as association–dissociation equilibria in solution with respect to different A-site cation combinations occurring in the solution-based processing of perovskite films is crucial to define parameters responsible for reproducible data. The experimentally obtained results must be interlinked with DFT calculations to establish and validate stable model systems along the entire value chain of modeling–synthesis–application (Fig. 7).

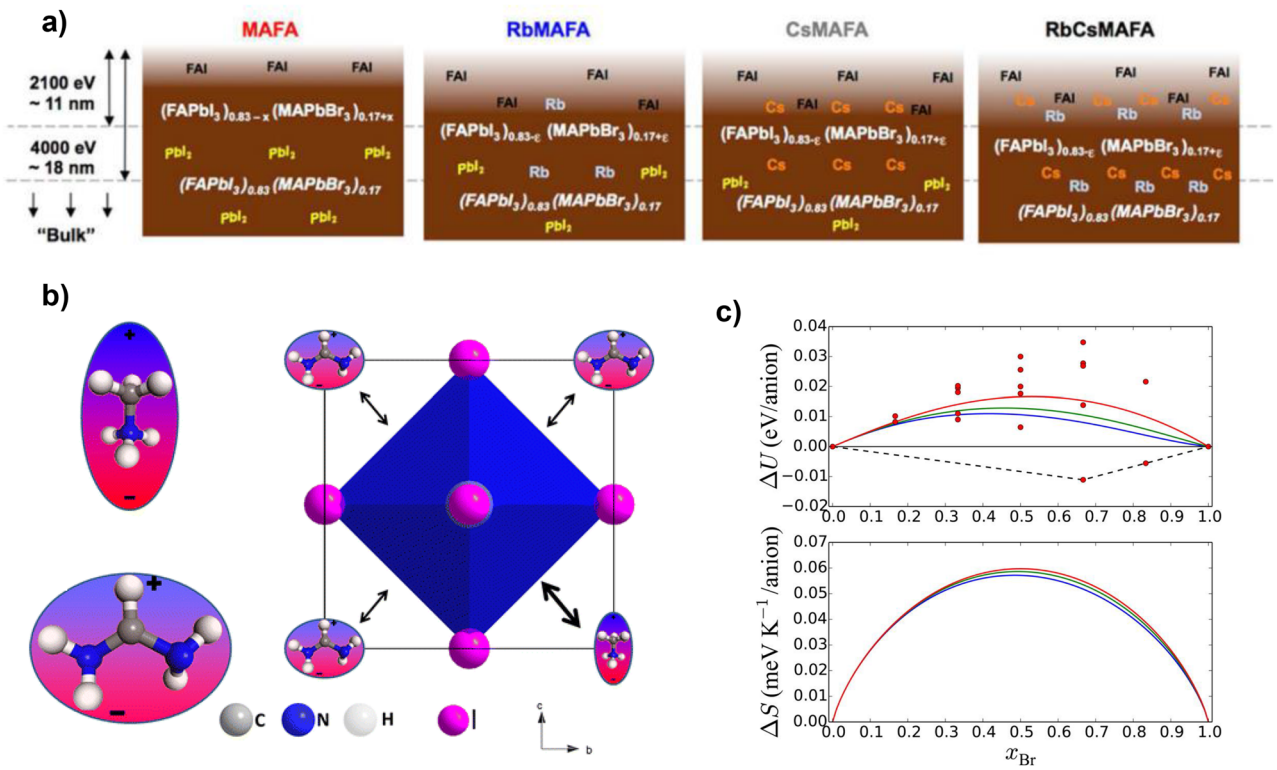

FIG. 6. (a) Distribution of the A-site cations in double-cation, triple-cation, and quadruple-cation perovskite thin-films. Reprinted with the permission from Philipe *et al.*, Chem. Mater. **29**, 3589 (2017). Copyright 2017 American Chemical Society. (b) Structure model of MA stabilized $FAPbI_3$ showing the different dipole moments and the impact on interaction within the perovskite lattice. Reprinted with permission from Binek *et al.*, J. Phys. Chem. Lett. **6**, 1249 (2015). Copyright 2015 American Chemical Society. (c) Diagrams showing energy of mixing and entropy of mixing for the $MAPb(I_{1-x}Br_x)_3$ alloy. Reprinted with permission from Brivio *et al.*, J. Phys. Chem. Lett. **7**, 1083 (2016). Copyright 2016 American Chemical Society .

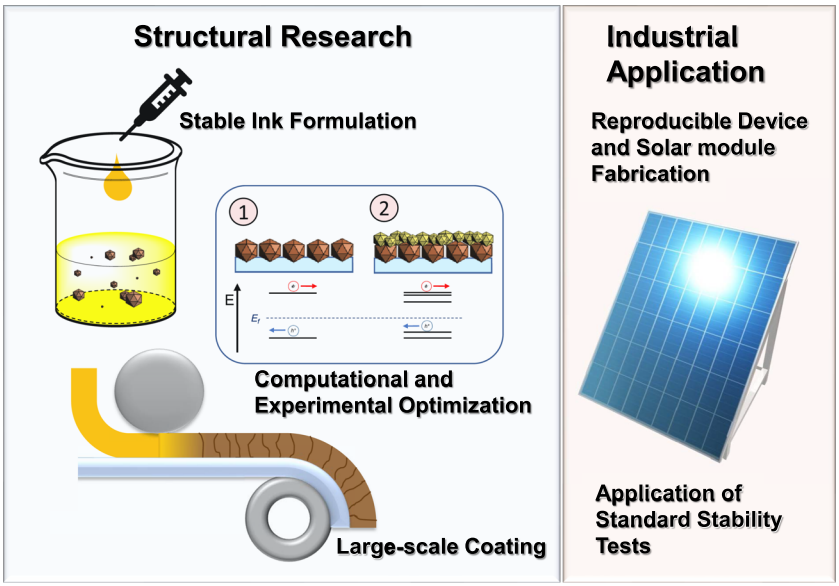

FIG. 7. Directions in research to achieve industrial application: building-up stable and well-understood hybrid perovskites via synthesis, modeling, and thin-film engineering. The goal is to achieve highly reproducible and stable solar devices tested by worldwide standardized procedures.

PROSPECTS FOR THEORETICAL INVESTIGATION OF MULTIPLE CATION PEROVSKITES

The theoretical understanding in the field of hybrid perovskites has been primarily revolving around electronic structure calculations based on density functional theory (DFT) formalism. The hidden electronic and optical properties of the hybrid perovskite family have been theoretically investigated to shed light on band structures, projected density of states, optical absorption spectra, and effective mass of charge carriers. The corresponding mobilities of the charge carriers can also be determined computationally to predict the electron–hole recombination rate. These electronic structure calculations are not only confined to the successful explanation of the efficiency and device stability of the corresponding hybrid perovskites materials but also manifested through the structural prediction and high-throughput screening. The ration screening based on the high throughput computation considers the cationic part, as well as the metal and halide counterpart, in different perovskite families, e.g., divalent, trivalent, and tetravalent metal-based perovskites and double perovskites (Fig. 8).

Another extension of such studies is the machine learning based theoretical prediction of structure–property relationships. However, the major drawback of such machine learning studies is the prediction accuracy while they correspond to the electronic structure calculations.[99] It is also inevitable to consider the relativistic spin orbit coupling effect in the DFT calculations[100–104] due to the presence of heavy elements like lead and bismuth in the perovskite systems. Moreover, the hybrid exchange correlation functional (HSE06) is known to provide a more accurate picture of the band structure and, particularly, the bandgap value.[105] The most pertinent effect can be observed in the Rashba–Dresselhaus phenomena.[106] These exciting phenomena are observed in the hybrid perovskite materials, where the splitting of the valence band maxima and conduction band minima is observed. This is originated from to the non-centrosymmetric crystal structure and relativistic spin orbit coupling effect due to the presence of a heavy element in the hybrid perovskite system.[107] The direct implications of the Rashba–Dresselhaus phenomena are observed in the charge carrier recombination process,[108,109] which is eventually getting delayed as the excited electrons temporarily stay in a newly created metastable conduction band due to the band splitting, rather than coming back directly to the valence band state.[110] Electronic structure calculations show that this effect can only be observed in non-centrosymmetric crystal structures if the SOC effect is considered. The disadvantage of less accurate electronic structure calculations can also be reflected in the phase transformation of the hybrid perovskite materials under the influence of temperature and pressure variation. Not considering the relativistic SOC effect and advanced hybrid exchange correlation functional might lead to the observation of a different space group, the phase in which the actual system does not belong.[107] The consequence of this influences the correspondence between theory and experimental observations, while governing the prediction of band structures, as the high symmetry path would be different and sensitive to a particular space group. The atomic arrangement in the hybrid perovskite systems is required to be as accurate as possible, as otherwise, it would lead to a different migration pathway for the constituent elements. The correct prediction of migration pathways in the hybrid perovskite materials is important, as it has been proposed that the hysteresis of the optoelectronic devices depends on such ion migrations.[46] Overall, the ongoing theoretical investigations have been proven instrumental for the successful explanation of the experimental observations, as well as the prediction of useful hybrid perovskite systems for the optoelectronic devices.

COMPOSITIONAL ENGINEERING FOR REDUCED RECOMBINATION LOSSES

Many publications on multiple-cation perovskites report on improved open-circuit voltages, increased luminescence efficiency,

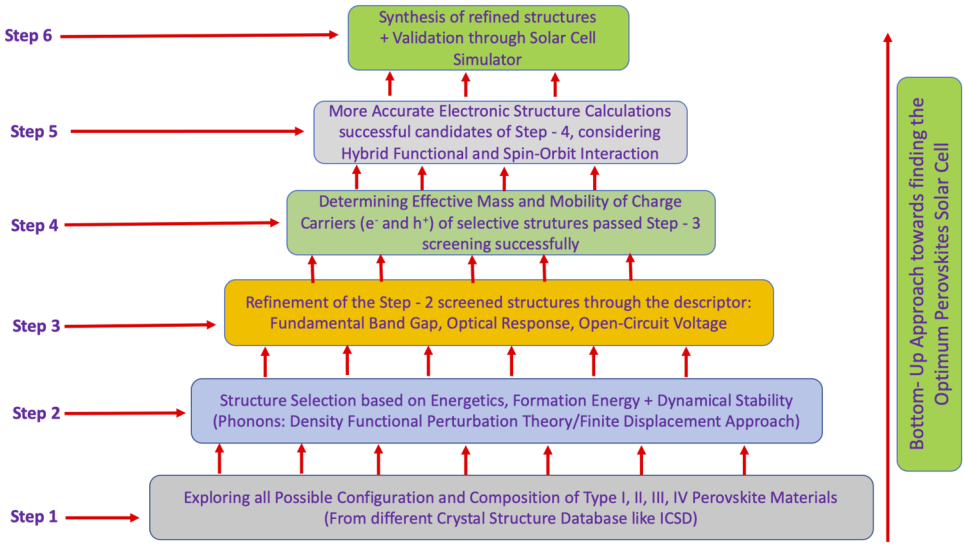

FIG. 8. High throughput screening of hybrid perovskite materials for efficient solar cells.

longer lifetimes, and reduced recombination losses relative to reference devices. However, few publications attempt to compare a larger range of perovskite compositions with respect to their ability to minimize non-radiative recombination losses. Comparative studies with a high level of film or device quality have been reported, e.g., by Feldmann *et al.*[111] and Stolterfoht *et al.*[112] Here, often, the luminescence quantum efficiency Q_e^{lum} is compared because it correlates with the maximum open-circuit voltage of a finished solar cell.[113] For a solar cell, we can correlate the two quantities via $V_{oc} = V_{oc,rad} + kT/q \times \ln(Q_e^{lum})$.[113] For a film on glass, the luminescence is generally higher than that for a solar cell,[114,115] and the difference between the values of Q_e^{lum} can be used to assess voltage losses due to recombination at the charge extracting interfaces of the device. Figure 9 a shows the photoluminescence quantum efficiency Q_e^{lum} measured on perovskite films with different stoichiometries as a function of excitation intensity to investigate the differences in the dominating bulk recombination kinetics. Figure 9 a shows a trend with the number of A-site cations, with more complicated compositions (incl., e.g., Rb and K) showing higher values of Q_e^{lum} and, hence, slower rate of non-radiative recombination processes.[111]

Comparable trends are seen in the data by Stolterfoht *et al.*[112] shown in Fig. 9(b). Here, the authors used light intensity-dependent PL measurements of neat films to construct an "ideal" current voltage curve including recombination losses in the bulk but excluding recombination losses at the interfaces to contact layers or any resistive losses. Figure 9(b) reports, for a range of compositions, both the value of the luminescence quantum efficiency and the efficiency (called pseudo-efficiency *pPCE* here) of the constructed J–V curves based on the PL of neat films. Again, the potassium containing perovskites show the highest *pPCE* and Q_e^{lum} implying the lowest non-radiative recombination losses in comparison to the other neat perovskite layers. In addition, also the different triple-cation compositions are generally better than the double-cation and single A-site cation compositions studied.

Figure 9(c), finally, shows a comparison of data extracted from high efficiency perovskite solar cells, reported in the literature. For a better comparison of parameters over a range of bandgaps, panel (c) shows efficiencies and efficiency losses relative to the values in the Shockley–Queisser limit. This type of loss analysis is described in more detail in Refs. 116 and 51 and is based on the idea that the normalized solar cell efficiency η/η_{SQ} can be written as a product of terms via[116]

$$\frac{\eta}{\eta_{SQ}} = F_{sc}\frac{V_{oc}FF_0(V_{oc})}{V_{oc}^{SQ}FF_0(V_{oc}^{SQ})}F_{FF}^{res}, \tag{5}$$

where $F_{SC} = J_{sc}/J_{sc}^{SQ}$ and F_{FF}^{res} represents the losses in *FF* due to series resistances and ideality factors $n_{id} > 1$. Every quantity with the superscript SQ is the respective quantity in the Shockley–Queisser limit, and every quantity without the subscript is the respective measured quantity of the actual solar cell. Here, FF_0 is the fill factor of an ideal solar cell without resistive losses and with an ideality factor $n_{id} = 1$. Figure 9(c) shows the losses on a logarithmic scale, which would allow us to change the order of the bars without having to change their size. Thereby, we can visualize the multiplicative terms in Eq. (1) in a sensible way. We observe that the main losses are due to the yellow, red, and green bars, which represent losses in J_{sc}, resistive and ideality factor losses in *FF*, and non-radiative recombination losses for V_{oc}. The latter losses shown in green should be the ones that most strongly correlate with Q_e^{lum}. However, we observe a different trend as compared to the situation with the neat films. Now, the lowest losses are achieved with either a double-cation composition[117] or even plain $MAPbI_3$.[15] In particular, the potassium containing solar cells show still low but substantially higher non-radiative recombination losses in devices as the two previously mentioned devices.[118] This observation suggests that so far, the potential of at least some of the more complex compositions has not been fully realized in complete devices. These additional recombination losses may be due to non-optimized interfaces to transport layers where more optimization has happened with simpler compositions. This suggests that higher efficiency may be possible in the future if these complex multi-cation compositions are combined with improved interfaces. In addition, we observe that a substantial amount of losses is indeed due to the imperfect fill factor caused mostly by the non-zero series resistance of contact layers. This loss is relatively stable over the different devices and suggests that further efficiency gains may be possible by improving the conductivity of the contact layers.[119]

PATH TOWARD COMMERCIALIZATION: OPPORTUNITIES AND BARRIERS

The solution-based fabrication of perovskite solar cell (PSC) absorber materials is established using a wide variety of deposition techniques,[120] such as single-step or sequential[121] deposition methods, via spin[122]-, dip[123]-, or vapor[124]-assisted coating techniques from mainly toxic solvents [i.e., dimethylformamide (DMF) and dimethyl sulfoxide (DMSO)].[125,126] To achieve widespread commercialization, this technology must address the responsible usage of toxic components like lead and solvents. Introducing protic ionic liquids (PILs) as solvent additives for perovskite solutions, green solvents such as water, ethyl alcohol, and isopropyl alcohol can be utilized for hybrid perovskite processing.[127] Thus, high boiling aprotic polar solvents can be replaced, and the range of applicable solvent candidates can be expanded, even toward water-based inks applied in general purpose desktop office ink-jet printers.[127] These PIL perovskite inks have high processing compatibility revealing the strong influence of the PIL anions (acetate and formate) on the solvation behavior of a lead (II) halide precursor;[127] nonetheless, achieving full homogeneous and smooth thin-films on large substrates remains challenging. The crystallization process is very sensitive toward applied solvents, concentrations, substrate morphologies, deposition times, and temperatures and even environmental conditions in different laboratories. Recently, newer deposition technologies have emerged for industrial application such as slot-die coating, screen printing, and other roll-to-roll technologies. However, these technologies must be optimized further to achieve the desired morphologies and suitable stabilities, as well as high efficiencies. Currently, there are few companies all over the world (Table II), which develop large-scale PSC modules: among them, in Europe, Oxford PV, one of the pioneering companies established by Prof. Henry Snaith from Oxford University, works on the commercialization of perovskite–silicon tandem photovoltaics, already achieving 28% for a 1 cm^2 device.[128] Saule Technologies located in Poland employs ink-jet printing of flexible perovskite solar cells with 10% PCE for solar modules (Fig. 10),[129] which

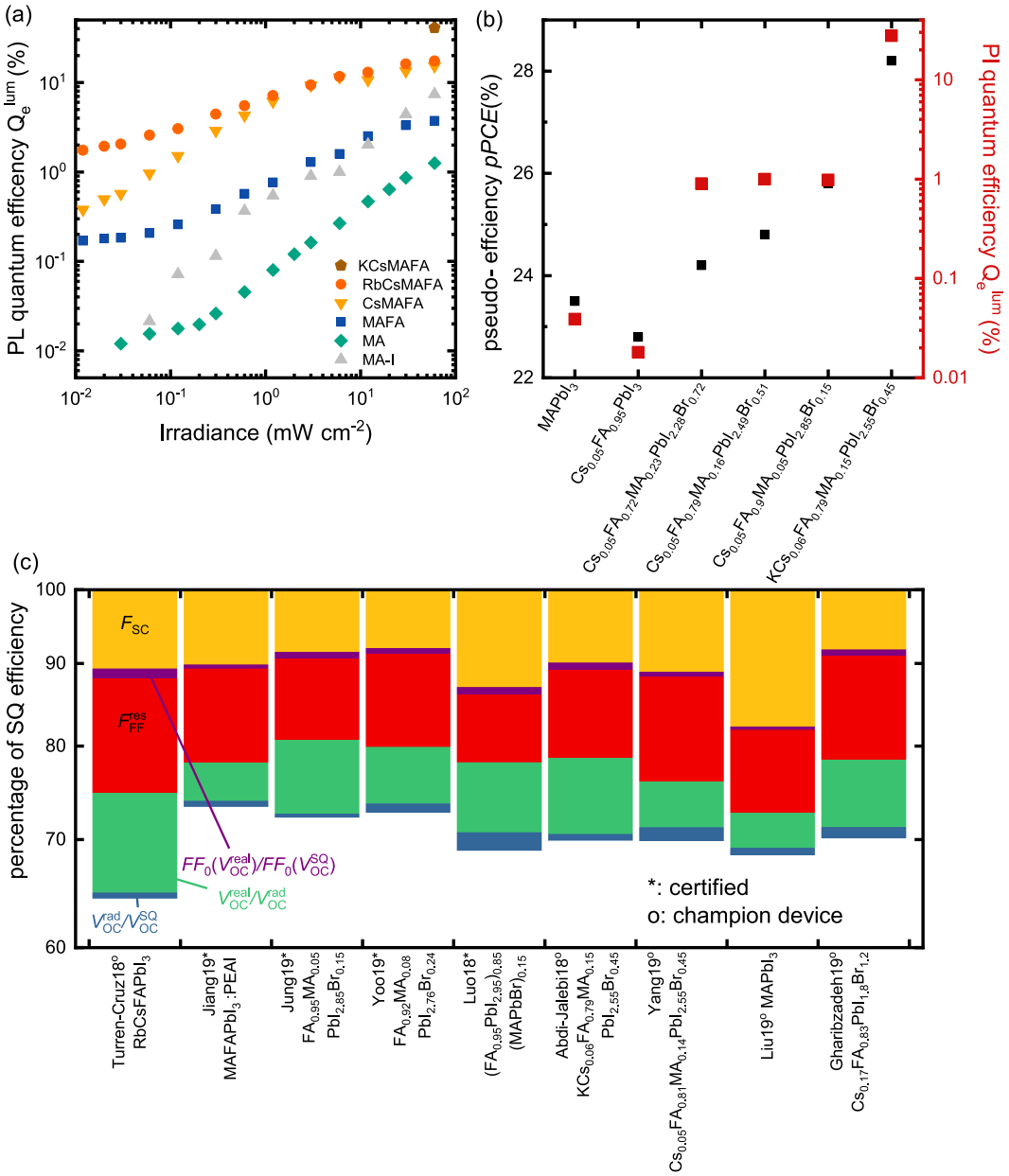

FIG. 9. (a) Fluence dependent photoluminescence quantum efficiency Q_e^{lum} measurement adopted from Feldmann *et al.*,[111] showing lower non-radiative recombination rates for mixed A-cite cations compared to single-cation perovskite and (b) pseudo-efficiency calculated from intensity-dependent PL measurements adapted from Stolterfoht *et al.*[112] for different mixtures of an A-cite cation perovskite without transport layers. In addition, for each sample, the photoluminescence quantum efficiency Q_e^{lum} of the corresponding perovskite layers is shown. (c) Illustration of the loss in J_{sc}, FF, and V_{oc} relative to the Shockley–Queisser limit[78] for high performing perovskite devices with different A-cite cation mixtures, displaying the various pathways for improvement of these devices. Panel (c) is copyright the authors of Ref. 51.

were recently installed in front of Henn na Hotel in Nagasaki, Japan.[130] Solliance in The Netherlands fabricates 169 cm^2 modules with 10% PCE based on a slot-die coating roll-to-roll process.[131] In China, Microquanta Semiconductor and Huazhong University of Science and Technology work on large area perovskite modules, with a PCE of 17.25% for a 19.2 cm^2 mini-module and 10% for a 100 cm^2 printable triple mesoscopic perovskite solar cells, respectively.[132] However, for many companies, the reported performances are the initial values and not tested for long-term stability.

TABLE II. Companies developing perovskite-based solar modules.

Company	Founded	Product	PCE and Scale	References
Toshiba	1875, Japan	Meniscus printed, lightweight, and flexible PSC	11.7% for 703 cm^2	133
Panasonic	1918, Japan	Rigid PSC	16.1% for 802 cm^2	3
Solaronix SA	1993, Switzerland	Building-integrated PSC	14.9% for 1 cm^2, 12% for 100 cm^2	134
Greatcell Solar (prev. Dyesol)	2004, Australia	On glass PSC	12% for 100 cm^2	132
Oxford PV	2010, UK	Perovskite/Si tandem SC	28% for 1 cm^2	128
Energy Materials Corp.	2010, US	Roll-to-roll coated PSC	Not published	134
Solliance	2010, The Netherlands	Slot-die coated PSC	10% for 16.75 cm^2	131
Saule Technologies	2014, Poland	Ink-jet printed flexible PSC	10% for solar modules, 17.6% cell level	129
Microquanta Semiconductor	2015, China	On glass PSC	17.25% for 19.2 cm^2	3 and 132
Wondersolar	2016, China	Screen-printed, triple mesoscopic PSC	110 m^2, PCE not published	132
Frontier Energy Sol.	2016, South Korea	Flexible and tandem SC	Not published	134
Tandem PV (prev. Iris PV)	2016, US	Perovskite/Si tandem SC	Not published	134
Swift Solar	2018, US	Flexible, lightweight PSC, and tandem SC	Not published	134

The attractivity of hybrid perovskites as an alternative to silicon or other thin-film technologies seems to be primarily due to their rapid development. Even if the companies mentioned above have started to use this absorber material in industry, the modules are still in an early phase of their development. One thing that is clear is that hybrid perovskites have actually made it from academic research laboratories to industrial development laboratories. Nevertheless, important insights into this innovative material

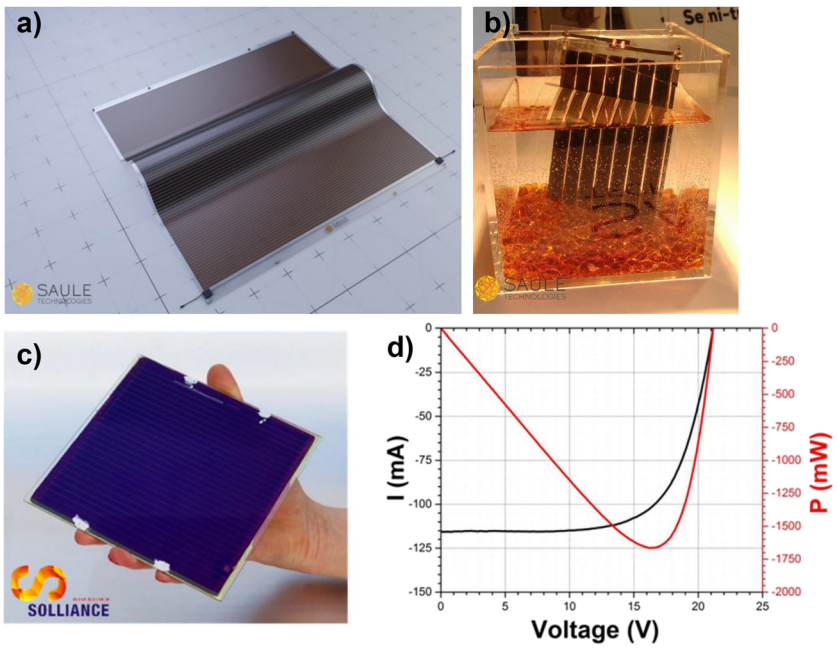

FIG. 10. (a) Flexible PSC developed in the laboratories of Saule Technologies. (b) Stability test against moisture of the PSC module by Saule Technologies. Photographs were kindly provided by Saule Technologies. Copyright Saule Tech. (c) Perovskite module (6 × 6 $in.^2$, by Solliance) and (d) the I–V curve with 10% PCE for the 168.75 cm^2 module. Reprinted with permission from Di Giacomo *et al.*, Sol. Energy Mater. Sol. Cells **181**, 53 (2018). Copyright 2018 Elsevier.

are missing, not only about its structural and chemical composition, as explained in the section titled "*Understanding the interplay of chemical structure and stability in mixed-cation perovskites*," but also its reproducibility. On the one hand, A-site cation engineering offers an opportunity to stabilize these hybrid perovskites and increase their efficiency. On the other hand, their precursor inks consist of a large number of components, whose real impact on crystallization has not yet been fully clarified. Furthermore, these inks must be stabilized, and their application to substrates must be optimized on an industrial scale. Ultimately, the perovskite must be able to prove itself under real conditions, such as exposure to higher or lower temperatures, rain, long operation times, and especially, shading from the environment, e.g., clouds, that it will cause reverse bias conditions in the shaded cells. All solar cells have a breakdown voltage, at which the current begins to flow in the reverse bias. If current flows in the reverse bias, the shaded cell consumes electricity instead of producing it, and this can cause local heating, which damages the cell.[135] Such local heating leads to degradation of the organic–inorganic hybrid perovskites due to the volatile organic components.[132] The resilience of solar cells under shading or a similar effect causing local heating is tested with hot spot endurance protocols (IEC 61215).[136] There are only a few studies that investigate perovskite solar cells in reverse bias conditions, which show reversible degradation of the perovskite, and damage on other parts of the device such as metal contacts.[135,136] In this context, it is important to further study the reverse bias conditions on perovskite solar cells and to develop robust solar cell design.[137] In summary, the desired maturity of PSC technology demands a judicious reduction of the parametric space of material synthesis and selection of materials based on their stress-tolerance and resilience under natural conditions (Fig. 11).

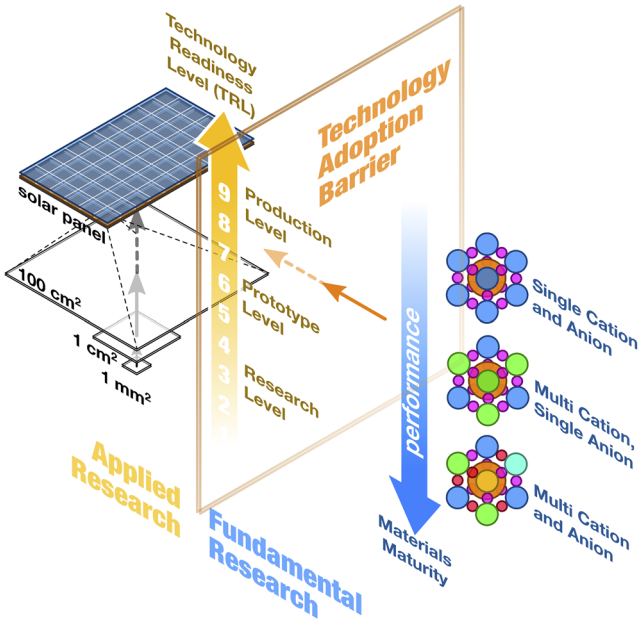

FIG. 11. PSC Technology at Crossroads: Schematic representation of the materials' readiness level that is affected by exploratory pathways for the materials' development and their maturity that does not always go hand in hand with the technology readiness level evaluated at the module level.

ACKNOWLEDGMENTS

F.Ü. and S.M. are grateful for the financial support from the German Science Foundation (DFG) provided in the framework of the priority program Grant No. SPP 2196, "Perovskite semiconductors: From fundamental properties to devices." J.H., A.K., and T.K. acknowledge support from the Helmholtz Association via the project PEROSEED.

Senol Öz declares competing interest, and the remaining authors take notice of it.

DATA AVAILABILITY

Data sharing is not applicable to this article as no new data were created or analyzed in this study.

REFERENCES

[1] T. Ibn-Mohammed, S. C. L. Koh, I. M. Reaney, A. Acquaye, G. Schileo, K. B. Mustapha, and R. Greenough, Renewable Sustainable Energy Rev. **80**, 1321 (2017).
[2] See https://www.nrel.gov/pp/cell-efficiency.html for NREL, 2020.
[3] M. A. Green, E. D. Dunlop, J. Hohl-Ebinger, M. Yoshita, N. Kopidakis, and A. W. Y. Ho-Baillie, Prog. Photovoltaics: Res. Appl. **28**, 3 (2020).
[4] H. J. Snaith, J. Phys. Chem. Lett. **4**, 3623–3630 (2013).
[5] A. Miyata, A. Mitioglu, P. Plochocka, O. Portugall, J. T.-W. Wang, S. D. Stranks, H. J. Snaith, and R. J. Nicholas, Nat. Phys. **11**, 582 (2015).
[6] J. Cui, H. Yuan, J. Li, X. Xu, Y. Shen, H. Lin, and M. Wang, Sci. Technol. Adv. Mater. **16**, 036004 (2015).
[7] M. Hirasawa, T. Ishihara, T. Goto, K. Uchida, and N. Miura, Physica B **201**, 427 (1994).
[8] V. D'Innocenzo, G. Grancini, M. J. P. Alcocer, A. R. S. Kandada, S. D. Stranks, M. M. Lee, G. Lanzani, H. J. Snaith, and A. Petrozza, Nat. Commun. **5**, 3586 (2014).
[9] D. A. Valverde-Chávez, C. S. Ponseca, C. C. Stoumpos, A. Yartsev, M. G. Kanatzidis, V. Sundström, and D. G. Cooke, Energy Environ. Sci. **8**, 3700 (2015).
[10] G. Xing, N. Mathews, S. Sun, S. S. Lim, Y. M. Lam, M. Grätzel, S. Mhaisalkar, and T. C. Sum, Science **6960**, 498 (2013).
[11] S. D. Stranks, G. E. Eperon, G. Grancini, C. Menelaou, M. J. P. Alcocer, T. Leijtens, L. M. Herz, A. Petrozza, and H. J. Snaith, Science **342**, 341 (2013).
[12] G. Giorgi, J.-I. Fujisawa, H. Segawa, and K. Yamashita, J. Phys. Chem. Lett. **4**, 4213 (2013).
[13] A. Kogo, Y. Sanehira, Y. Numata, M. Ikegami, and T. Miyasaka, ACS Appl. Mater. Interfaces **10**, 2224 (2018).
[14] Y. Li, R. L. Z. Hoye, H.-H. Gao, L. Yan, X. Zhang, Y. Zhou, J. L. MacManus-Driscoll, and J. Gan, ACS Appl. Mater. Interfaces **12**, 7135 (2020).
[15] Z. Liu, L. Krückemeier, B. Krogmeier, B. Klingebiel, J. A. Márquez, S. Levcenko, S. Öz, S. Mathur, U. Rau, T. Unold, and T. Kirchartz, ACS Energy Lett. **4**, 110 (2019).
[16] J. Cao, B. Wu, R. Chen, Y. Wu, Y. Hui, B. W. Mao, and N. Zheng, Adv. Mater. **30**, 1705596 (2018).
[17] G. Niu, X. Guo, and L. Wang, J. Mater. Chem. A **3**, 8970 (2015).
[18] T. T. Ava, A. Al Mamun, S. Marsillac, and G. Namkoong, Appl. Sci. **9**, 188 (2019).
[19] N. Aristidou, I. Sanchez-Molina, T. Chotchuangchutchaval, M. Brown, L. Martinez, T. Rath, and S. A. Haque, Angew. Chem., Int. Ed. **54**, 8208 (2015).
[20] G. Niu, W. Li, F. Meng, L. Wang, H. Dong, and Y. Qiu, J. Mater. Chem. A **2**, 705 (2014).
[21] S. Ito, S. Tanaka, K. Manabe, and H. Nishino, J. Phys. Chem. C **118**, 16995 (2014).

[22]N. Onoda-Yamamuro, T. Matsuo, and H. Suga, J. Phys. Chem. Solids **51**, 1383 (1990).
[23]T. Baikie, Y. Fang, J. M. Kadro, M. Schreyer, F. Wei, S. G. Mhaisalkar, M. Graetzel, and T. J. White, J. Mater. Chem. A **1**, 5628 (2013).
[24]T. A. Berhe, W.-N. Su, C.-H. Chen, C.-J. Pan, J.-H. Cheng, H.-M. Chen, M.-C. Tsai, L.-Y. Chen, A. A. Dubale, and B.-J. Hwang, Energy Environ. Sci. **9**, 323 (2016).
[25]A. F. Akbulatov, L. A. Frolova, N. N. Dremova, I. Zhidkov, V. M. Martynenko, S. A. Tsarev, S. Y. Luchkin, E. Z. Kurmaev, S. M. Aldoshin, K. J. Stevenson, and P. A. Troshin, J. Phys. Chem. Lett. **11**, 333 (2020).
[26]N. J. Jeon, J. H. Noh, W. S. Yang, Y. C. Kim, S. Ryu, J. Seo, and S. I. Seok, Nature **517**, 476 (2015).
[27]G. E. Eperon, S. D. Stranks, C. Menelaou, M. B. Johnston, L. M. Herz, and H. J. Snaith, Energy Environ. Sci. **7**, 982 (2014).
[28]D. M. Trots and S. V. Myagkota, J. Phys. Chem. Solids **69**, 2520 (2008).
[29]H. Tsai, W. Nie, J.-C. Blancon, C. C. Stoumpos, R. Asadpour, B. Harutyunyan, A. J. Neukirch, R. Verduzco, J. J. Crochet, S. Tretiak, L. Pedesseau, J. Even, M. A. Alam, G. Gupta, J. Lou, P. M. Ajayan, M. J. Bedzyk, M. G. Kanatzidis, and A. D. Mohite, Nature **536**, 312 (2016).
[30]I. C. Smith, E. T. Hoke, D. Solis-Ibarra, M. D. McGehee, and H. I. Karunadasa, Angew. Chem., Int. Ed. **53**, 11232 (2014).
[31]G. Grancini, C. Roldán-Carmona, I. Zimmermann, E. Mosconi, X. Lee, D. Martineau, S. Narbey, F. Oswald, F. De Angelis, M. Graetzel, and M. K. Nazeeruddin, Nat. Commun. **8**, 15684 (2017).
[32]B. Chen, P. N. Rudd, S. Yang, Y. Yuan, and J. Huang, Chem. Soc. Rev. **48**, 3842 (2019).
[33]T. W. Jones, A. Osherov, M. Alsari, M. Sponseller, B. C. Duck, Y.-K. Jung, C. Settens, F. Niroui, R. Brenes, C. V. Stan, Y. Li, M. Abdi-Jalebi, N. Tamura, J. E. MacDonald, M. Burghammer, R. H. Friend, V. Bulović, A. Walsh, G. J. Wilson, S. Lilliu, and S. D. Stranks, Energy Environ. Sci. **12**, 596 (2019).
[34]J. M. Ball and A. Petrozza, Nat. Energy **1**, 16149 (2016).
[35]H. Jin, E. Debroye, M. Keshavarz, I. G. Scheblykin, M. B. J. Roeffaers, J. Hofkens, and J. A. Steele, Mater. Horiz. **7**, 397 (2020).
[36]V. M. Goldschmidt, Naturwissenschaften **14**, 477 (1926).
[37]C. Li, X. Lu, W. Ding, L. Feng, Y. Gao, and Z. Guo, Acta Crystallogr., Sect. B: Struct. Sci. **64**, 702 (2008).
[38]M. Johnsson and P. Lemmens, Handb. Magn. Adv. Magn. Mater. **4**, 1 (2007).
[39]G. Kieslich, S. Sun, and A. K. Cheetham, Chem. Sci. **6**, 3430 (2015).
[40]Z. Li, M. Yang, J.-S. Park, S.-H. Wei, J. J. Berry, and K. Zhu, Chem. Mater. **28**, 284 (2016).
[41]T. Umebayashi, K. Asai, T. Kondo, and A. Nakao, Phys. Rev. B **67**, 155405 (2003).
[42]J. J. Yoo, S. Wieghold, M. C. Sponseller, M. R. Chua, S. N. Bertram, N. T. P. Hartono, J. S. Tresback, E. C. Hansen, J.-P. Correa-Baena, V. Bulović, T. Buonassisi, S. S. Shin, and M. G. Bawendi, Energy Environ. Sci. **12**, 2192 (2019).
[43]R. Roesch, T. Faber, E. Von Hauff, T. M. Brown, M. Lira-Cantu, and H. Hoppe, Adv. Energy Mater. **5**, 1501407 (2015).
[44]N.-G. Park and H. Segawa, ACS Photonics **5**, 2970 (2018).
[45]L. Meng, J. You, and Y. Yang, Nat. Commun. **9**, 5265 (2018).
[46]P. Liu, W. Wang, S. Liu, H. Yang, and Z. Shao, Adv. Energy Mater. **9**, 1803017 (2019).
[47]W. Tress, N. Marinova, T. Moehl, S. M. Zakeeruddin, M. K. Nazeeruddin, and M. Grätzel, Energy Environ. Sci. **8**, 995 (2015).
[48]F. Arabpour Roghabadi, M. Alidaei, S. M. Mousavi, T. Ashjari, A. S. Tehrani, V. Ahmadi, and S. M. Sadrameli, J. Mater. Chem. A **7**, 5898 (2019).
[49]A. Binek, F. C. Hanusch, P. Docampo, and T. Bein, J. Phys. Chem. Lett. **6**, 1249 (2015).
[50]T. M. Koh, K. Fu, Y. Fang, S. Chen, T. C. Sum, N. Mathews, S. G. Mhaisalkar, P. P. Boix, and T. Baikie, J. Phys. Chem. C **118**, 16458 (2014).
[51]L. Krückemeier, U. Rau, M. Stolterfoht, and T. Kirchartz, Adv. Energy Mater. **10**, 1902573 (2020).
[52]Y. Zhang, S. Seo, S. Y. Lim, Y. Kim, S. G. Kim, D. K. Lee, S. H. Lee, H. Shin, H. Cheong, and N. G. Park, ACS Energy Lett. **5**, 360 (2020).
[53]Z. Li, F. Zhou, Q. Wang, L. Ding, and Z. Jin, Nano Energy **71**, 104634 (2020).
[54]Y. Wang, X. Liu, T. Zhang, X. Wang, M. Kan, J. Shi, and Y. Zhao, Angew. Chem., Int. Ed. **58**, 16691 (2019).
[55]C. Caetano, K. T. Butler, and A. Walsh, Phys. Rev. B **93**, 144205 (2016).
[56]C. Yi, J. Luo, S. Meloni, A. Boziki, N. Ashari-Astani, C. Grätzel, S. M. Zakeeruddin, U. Röthlisberger, and M. Grätzel, Energy Environ. Sci. **9**, 656 (2016).
[57]K. T. Butler, A. Walsh, A. K. Cheetham, and G. Kieslich, Chem. Sci. **7**, 6316 (2016).
[58]N. Pellet, P. Gao, G. Gregori, T.-Y. Yang, M. K. Nazeeruddin, J. Maier, and M. Grätzel, Angew. Chem., Int. Ed. **53**, 3151 (2014).
[59]M. V. Fedotova and S. E. Kruchinin, Russ. Chem. Bull. **61**, 240 (2012).
[60]B. Conings, J. Drijkoningen, N. Gauquelin, A. Babayigit, J. D'Haen, L. D'Olieslaeger, A. Ethirajan, J. Verbeeck, J. Manca, E. Mosconi, F. De Angelis, and H. G. Boyen, Adv. Energy Mater. **5**, 1500477 (2015).
[61]X. Wu, Y. Jiang, C. Chen, J. Guo, X. Kong, Y. Feng, S. Wu, X. Gao, X. Lu, Q. Wang, G. Zhou, Y. Chen, J.-M. Liu, K. Kempa, and J. Gao, Adv. Funct. Materials **30**(6), 1908613 (2020).
[62]J. W. Lee, D. H. Kim, H. S. Kim, S. W. Seo, S. M. Cho, and N. G. Park, Adv. Energy Mater. **5**, 1501310 (2015).
[63]N. Li, J. Liu, C. Li, Y. Li, J. Jia, Y. Wu, H. Yu, B. Yuan, and B. Cao, ACS Sustainable Chem. Eng. **8**, 7020 (2020).
[64]D. P. McMeekin, G. Sadoughi, W. Rehman, G. E. Eperon, M. Saliba, M. T. Hörantner, A. Haghighirad, N. Sakai, L. Korte, B. Rech, M. B. Johnston, L. M. Herz, and H. J. Snaith, Science **351**, 151 (2016).
[65]M. H. Futscher and B. Ehrler, ACS Energy Lett. **1**, 863 (2016).
[66]Y. Zhang, G. Grancini, Y. Feng, A. M. Asiri, and M. K. Nazeeruddin, ACS Energy Lett. **2**, 802 (2017).
[67]E. H. Jung, N. J. Jeon, E. Y. Park, C. S. Moon, T. J. Shin, T.-Y. Yang, J. H. Noh, and J. Seo, Nature **567**, 511 (2019).
[68]N. J. Jeon, H. Na, E. H. Jung, T.-Y. Yang, Y. G. Lee, G. Kim, H.-W. Shin, S. Il Seok, J. Lee, and J. Seo, Nat. Energy **3**, 682 (2018).
[69]M. Saliba, T. Matsui, J.-Y. Y. Seo, K. Domanski, J.-P. Correa-Baena, M. K. Nazeeruddin, S. M. Zakeeruddin, W. Tress, A. Abate, A. Hagfeldt, M. Grätzel, M. K. Nazeeruddin, S. M. Zakeeruddin, W. Tress, A. Abate, A. Hagfeldt, and M. Grätzel, Energy Environ. Sci. **9**, 1989 (2016).
[70]M. Saliba, T. Matsui, K. Domanski, J.-Y. Seo, A. Ummadisingu, S. M. Zakeeruddin, J.-P. Correa-Baena, W. Tress, A. Abate, A. Hagfeldt, and M. Grätzel, Science **354**, 206 (2016).
[71]T. Bu, X. Liu, Y. Zhou, J. Yi, X. Huang, L. Luo, J. Xiao, Z. Ku, Y. Peng, F. Huang, Y.-B. Cheng, and J. Zhong, Energy Environ. Sci. **10**, 2509 (2017).
[72]E. Jung, K. Budzinauskas, S. Öz, F. Ünlü, H. Kuhn, J. Wagner, D. Grabowski, B. Klingebiel, M. Cherasse, J. Dong, P. Aversa, P. Vivo, T. Kirchartz, T. Miyasaka, P. H. M. Van Loosdrecht, L. Perfetti, and S. Mathur, ACS Energy Lett. **5**, 785 (2020).
[73]Y. H. Park, I. Jeong, S. Bae, H. J. Son, P. Lee, J. Lee, C. H. Lee, and M. J. Ko, Adv. Funct. Mater. **27**, 1605988 (2017).
[74]D. J. Kubicki, D. Prochowicz, A. Hofstetter, S. M. Zakeeruddin, M. Grätzel, and L. Emsley, J. Am. Chem. Soc. **139**, 14173 (2017).
[75]N. De Marco, H. Zhou, Q. Chen, P. Sun, Z. Liu, L. Meng, E.-P. Yao, Y. Liu, A. Schiffer, and Y. Yang, Nano Lett. **16**, 1009 (2016).
[76]A. D. Jodlowski, C. Roldán-Carmona, G. Grancini, M. Salado, M. Ralaiarisoa, S. Ahmad, N. Koch, L. Camacho, G. De Miguel, and M. K. Nazeeruddin, Nat. Energy **2**, 972 (2017).
[77]S. Wu, Z. Li, J. Zhang, T. Liu, Z. Zhu, and A. K.-Y. Jen, Chem. Commun. **55**, 4315 (2019).
[78]W. Shockley and H. J. Queisser, J. Appl. Phys. **32**, 510 (1961).
[79]T. Kirchartz and U. Rau, Adv. Energy Mater. **8** (2018).
[80]T. Singh and T. Miyasaka, Adv. Energy Mater. **8**, 1700677 (2018).
[81]T. Matsui, T. Yokoyama, T. Negami, T. Sekiguchi, M. Saliba, M. Grätzel, and H. Segawa, Chem. Lett. **47**, 814 (2018).
[82]J. Cao, S. X. Tao, P. A. Bobbert, C. P. Wong, and N. Zhao, Adv. Mater. **30**, 1707350 (2018).

[83]M. Abdi-Jalebi, Z. Andaji-Garmaroudi, A. J. Pearson, G. Divitini, S. Cacovich, B. Philippe, H. Rensmo, C. Ducati, R. H. Friend, and S. D. Stranks, ACS Energy Lett. **3**, 2671 (2018).
[84]W. Zhang, J. Xiong, J. Li, and W. A. Daoud, J. Mater. Chem. A **7**, 9486 (2019).
[85]B. Cao, L. Yang, S. Jiang, H. Lin, N. Wang, and X. Li, J. Mater. Chem. A **7**, 4960 (2019).
[86]A. Amat, E. Mosconi, E. Ronca, C. Quarti, P. Umari, M. K. Nazeeruddin, M. Grätzel, and F. De Angelis, Nano Lett. **14**, 3608 (2014).
[87]A. K. Jena, A. Kulkarni, and T. Miyasaka, Chem. Rev. **119**, 3036 (2019).
[88]P. Zhao, W. Yin, M. Kim, M. Han, Y. J. Song, T. K. Ahn, and H. S. Jung, J. Mater. Chem. A **5**, 7905 (2017).
[89]D. J. Kubicki, D. Prochowicz, A. Hofstetter, S. M. Zakeeruddin, M. Grätzel, and L. Emsley, J. Am. Chem. Soc. **140**, 7232 (2018).
[90]G. Zhou, J. Wu, Y. Zhao, Y. Li, J. Shi, Y. Li, H. Wu, D. Li, Y. Luo, and Q. Meng, ACS Appl. Mater. Interfaces **10**, 9503 (2018).
[91]W. Jian, R. Jia, H.-X. Zhang, and F.-Q. Bai, Inorg. Chem. Front. **7**, 1741 (2020).
[92]B. Philippe, M. Saliba, J.-P. Correa-Baena, U. B. Cappel, S.-H. Turren-Cruz, M. Grätzel, A. Hagfeldt, and H. Rensmo, Chem. Mater. **29**, 3589 (2017).
[93]J.-W. Yeh, S.-K. Chen, S.-J. Lin, J.-Y. Gan, T.-S. Chin, T.-T. Shun, C.-H. Tsau, and S.-Y. Chang, Adv. Eng. Mater. **6**, 299 (2004).
[94]H.-W. Luan, Y. Shao, J.-F. Li, W.-L. Mao, Z.-D. Han, C. Shao, and K.-F. Yao, Scr. Mater. J. **179**, 40 (2020).
[95]F. Brivio, C. Caetano, and A. Walsh, J. Phys. Chem. Lett. **7**, 1083 (2016).
[96]E. T. Hoke, D. J. Slotcavage, E. R. Dohner, A. R. Bowring, H. I. Karunadasa, and M. D. McGehee, Chem. Sci. **6**, 613 (2015).
[97]E. L. Unger, L. Kegelmann, K. Suchan, D. Sörell, L. Korte, and S. Albrecht, J. Mater. Chem. A **5**, 011401 (2017).
[98]K. Suchan, A. Merdasa, C. Rehermann, E. L. Unger, and I. G. Scheblykin, J. Lumin. **221**, 117073 (2020).
[99]G. R. Schleder, A. C. M. Padilha, C. M. Acosta, M. Costa, and A. Fazzio, J. Phys. Mater. **2**, 032001 (2019).
[100]S. Bera, D. Ghosh, A. Dutta, S. Bhattacharyya, S. Chakraborty, and N. Pradhan, ACS Energy Lett. **4**, 1364 (2019).
[101]H. Arfin, J. Kaur, T. Sheikh, S. Chakraborty, and A. Nag, Angew. Chem., Int. Ed. **59**, 1–6 (2020).
[102]A. Banerjee, S. Chakraborty, and R. Ahuja, J. Mater. Chem. A **5**, 18561 (2017).
[103]S. Krishnamurthy, R. Naphade, W. J. Mir, S. Gosavi, S. Chakraborty, R. Vaidhyanathan, and S. Ogale, Adv. Opt. Mater. **6**, 1800751 (2018).
[104]S. Parmar, S. Pal, A. Biswas, S. Gosavi, S. Chakraborty, M. C. Reddy, and S. Ogale, Chem. Commun. **55**, 7562 (2019).
[105]D. I. Bilc, R. Orlando, R. Shaltaf, G. M. Rignanese, J. Íñiguez, and P. Ghosez, Phys. Rev. B **77**, 165107 (2008).
[106]A. Banerjee, S. Chakraborty, and R. Ahuja, ACS Appl. Energy Mater. **2**, 6990 (2019).
[107]J. Even, L. Pedesseau, J.-M. Jancu, and C. Katan, J. Phys. Chem. Lett. **4**, 2999 (2013).
[108]T. Etienne, E. Mosconi, and F. De Angelis, J. Phys. Chem. Lett. **7**, 1638 (2016).
[109]A. Maiti, S. Khatun, and A. J. Pal, Nano Lett. **20**, 292 (2020).
[110]M. Kepenekian, R. Robles, C. Katan, D. Sapori, L. Pedesseau, and J. Even, ACS Nano **9**, 11557 (2015).
[111]S. Feldmann, S. Macpherson, S. P. Senanayak, M. Abdi-Jalebi, J. P. H. Rivett, G. Nan, G. D. Tainter, T. A. S. Doherty, K. Frohna, E. Ringe, R. H. Friend, H. Sirringhaus, M. Saliba, D. Beljonne, S. D. Stranks, and F. Deschler, Nat. Photonics **14**, 123 (2020).
[112]M. Stolterfoht, M. Grischek, P. Caprioglio, C. M. Wolff, E. Gutierrez-Partida, F. Peña-Camargo, D. Rothhardt, S. Zhang, M. Raoufi, J. Wolansky, M. Abdi-Jalebi, S. D. Stranks, S. Albrecht, T. Kirchartz, and D. Neher, Adv. Mater. **32**, 2000080 (2020).
[113]U. Rau, Phys. Rev. B **76**, 085303 (2007).
[114]M. Stolterfoht, P. Caprioglio, C. M. Wolff, J. A. Márquez, J. Nordmann, S. Zhang, D. Rothhardt, U. Hörmann, Y. Amir, A. Redinger, L. Kegelmann, F. Zu, S. Albrecht, N. Koch, T. Kirchartz, M. Saliba, T. Unold, and D. Neher, Energy Environ. Sci. **12**, 2778 (2019).
[115]E. M. Hutter, T. Kirchartz, B. Ehrler, D. Cahen, and E. Von Hauff, Appl. Phys. Lett. **116**, 100501 (2020).
[116]J.-F. Guillemoles, T. Kirchartz, D. Cahen, and U. Rau, Nat. Photonics **13**, 501 (2019).
[117]Q. Jiang, Y. Zhao, X. Zhang, X. Yang, Y. Chen, Z. Chu, Q. Ye, X. Li, Z. Yin, and J. You, Nat. Photonics **13**, 460 (2019).
[118]M. Abdi-Jalebi, Z. Andaji-Garmaroudi, S. Cacovich, C. Stavrakas, B. Philippe, J. M. Richter, M. Alsari, E. P. Booker, E. M. Hutter, A. J. Pearson, S. Lilliu, T. J. Savenije, H. Rensmo, G. Divitini, C. Ducati, R. H. Friend, and S. D. Stranks, Nature **555**, 497 (2018).
[119]V. M. Le Corre, M. Stolterfoht, L. Perdigón Toro, M. Feuerstein, C. Wolff, L. Gil-Escrig, H. J. Bolink, D. Neher, and L. J. A. Koster, ACS Appl. Energy Mater. **2**, 6280 (2019).
[120]Z. Li, T. R. Klein, D. H. Kim, M. Yang, J. J. Berry, M. F. A. M. Van Hest, and K. Zhu, Nat. Rev. Mater. **3**, 18017 (2018).
[121]J. Burschka, N. Pellet, S.-J. Moon, R. Humphry-Baker, P. Gao, M. K. Nazeeruddin, and M. Grätzel, Nature **499**, 316 (2013).
[122]J. H. Heo, D. H. Song, and S. H. Im, Adv. Mater. **26**, 8179 (2014).
[123]M. Adnan and J. K. Lee, Sci. Rep. **8**, 2168 (2018).
[124]M. Liu, M. B. Johnston, and H. J. Snaith, Nature **501**, 395 (2013).
[125]Y. Rong, Z. Tang, Y. Zhao, X. Zhong, S. Venkatesan, H. Graham, M. Patton, Y. Jing, A. M. Guloy, and Y. Yao, Nanoscale **7**, 10595 (2015).
[126]N. J. Jeon, J. H. Noh, Y. C. Kim, W. S. Yang, S. Ryu, and S. Il Seok, Nat. Mater. **13**, 897 (2014).
[127]S. Öz, J. Burschka, E. Jung, R. Bhattacharjee, T. Fischer, A. Mettenbörger, H. Wang, and S. Mathur, Nano Energy **51**, 632 (2018).
[128]T. Sherahilo, https://www.oxfordpv.com/news/oxford-pv-perovskite-solar-cell-achieves-28-efficiency (2018).
[129]G. Auverton, https://www.laserfocusworld.com/detectors-imaging/article/14035450/saule-prints-flexible-perovskite-solar-modules-with-consistent-10-efficiency (2019).
[130]See https://sauletech.com/saule-perovskite-solar-panel-in-the-worlds-most-innovative-hotel/ for Saule Technologies, 2018.
[131]F. Di Giacomo, S. Shanmugam, H. Fledderus, B. J. Bruijnaers, W. J. H. Verhees, M. S. Dorenkamper, S. C. Veenstra, W. Qiu, R. Gehlhaar, T. Merckx, T. Aernouts, R. Andriessen, and Y. Galagan, Sol. Energy Mater. Sol. Cells **181**, 53 (2018).
[132]Y. Rong, Y. Hu, A. Mei, H. Tan, M. I. Saidaminov, S. Il Seok, M. D. McGehee, E. H. Sargent, and H. Han, Science **361**, eaat8235 (2018).
[133]See https://www.toshiba.co.jp/rdc/rd/detail_e/e1806_03.html for information about Nedo and Toshiba's large-scale Perovskite Photovoltaic Module, 2018.
[134]A. Extance, Springer Nat **570**, 429 (2019).
[135]A. R. Bowring, L. Bertoluzzi, B. C. O'Regan, and M. D. McGehee, Adv. Energy Mater. **8**, 1702365 (2018).
[136]P. Holzhey and M. Saliba, J. Mater. Chem. A **6**, 21794 (2018).
[137]R. A. Z. Razera, D. A. Jacobs, F. Fu, P. Fiala, M. Dussouillez, F. Sahli, T. C. J. Yang, L. Ding, A. Walter, A. F. Feil, H. I. Boudinov, S. Nicolay, C. Ballif, and Q. Jeangros, J. Mater. Chem. A **8**, 242 (2019).